International Journal of Minerals, Metallurgy and Materials
Volume 23, Number 1, January 2016, Page 102
DOI: 10.1007/s12613-016-1216-1

Structural, morphological, Raman, optical, magnetic, and antibacterial characteristics of CeO_2 nanostructures

Fazal Abbas[1)], *Javed Iqbal*[1)], *Tariq Jan*[1)], *Noor Badshah*[2)], *Qaisar Mansoor*[3)], *and Muhammad Ismail*[3)]

1) Laboratory of Nanoscience and Technology, Department of Physics, International Islamic University, H-10, Islamabad 44000, Pakistan

2) Department of Basic Science, University of Engineering and Technology, Peshawar 26000, Pakistan

3) Institute of Biomedical and Genetic Engineering (IBGE), Islamabad 44000, Pakistan

(Received: 25 March 2015; revised: 3 July 2015; accepted: 6 July 2015)

Abstract: In this study, CeO_2 nanostructures were synthesized by a soft chemical method. A hydrothermal treatment was observed to lead to an interesting morphological transformation of the nanoparticles into homogeneous microspheres composed of nanosheets with an average thickness of 40 nm. Structural analysis revealed the formation of a single-phase cubic fluorite structure of CeO_2 for both samples. A Raman spectroscopic study confirmed the XRD results and furthermore indicated the presence of a large number of oxygen vacancies in the nanosheets. These oxygen vacancies led to room-temperature ferromagnetism (RTFM) of the CeO_2 nanosheets with enhanced magnetic characteristics. Amazingly, the nanosheets exhibited substantially greater antibacterial activity than the nanoparticles. This greater antibacterial activity was attributed to greater exposure of high-surface-energy polar surfaces and to the presence of oxygen vacancies.

Keywords: cecium oxide; nanosheets; chemical synthesis; ferromagnetism; oxygen vacancies; antibacterial properties

1. Introduction

CeO_2 is a fascinating material that is widely used in various industrial products such as polishing agents, sunscreens (as a UV-absorbing material), solid-oxide fuel cells (as an electrolyte), photocatalysts, and humidity sensors [1–3]. CeO_2 nanostructures have attracted extensive attention because of their antioxidant properties, ability to prevent induced pneumonitis, ability to inhibit bacteria, anticancer activity, and ability to protect living cells against radiation [3–5]. However, the functionalities of these CeO_2-nanostructure-based devices strictly depend on the particle size and morphology of the CeO_2 [6–7]. Methods such as chemical co-precipitation, sol–gel, chemical vapor deposition, and hydrothermal techniques are currently being used to fabricate CeO_2 nanostructures with controlled morphology [4–8]. Among these techniques, soft chemical routes are preferred because they are cost effective, versatile, vibrant, and easily reproduced. Moreover, because of its unfilled 4f electronic structure, CeO_2 exhibits interesting spintronic, electronic, and magnetic properties [4].

Room-temperature ferromagnetism (RTFM) is essential requirement for the functionality of spintronics devices. RTFM has been reported to be induced in various semiconductor metal oxides via transition-metal doping [9–11]. The real cause of this ferromagnetic behavior is ambiguous and is linked to various factors such as magnetic dopant clusters in oxide matrices, the valence states of the transition metals, the size and shape of the particles, and the presence of oxygen vacancies [12–13]. However, some authors have reported RTFM in pure metal oxide nanostructures such as those of ZnO, TiO_2, CuO_2, SnO_2, and CeO_2 [9–12, 14]. This RTFM is associated strictly with particle size and oxygen vacancies [15–16]. Liu *et al.* [13] recently reported that oxygen vacancies are not necessary for RTFM of undoped CeO_2 nanostructures and that particle size is instead the key factor. However, Ge *et al.* [12] reported that oxygen vacancies are responsible for the ferromagnetic behavior of CeO_2 nanocubes. In this work, we have synthesized CeO_2 nanostructures with an average particle size of 30–40 nm and different morphologies. Interestingly, we observed that oxygen vacancies play a major role in the RTFM of these CeO_2

Corresponding author: Tariq Jan E-mail: tariqjan84@gmail.com

nanostructures.

2. Materials and methods

2.1. Synthesis of CeO_2 nanostructures

CeO_2 nanostructures were prepared by a facile soft chemical route. A 0.2 M $Ce(NO_3)_3{\cdot}6H_2O$ solution was prepared in deionized water. Sufficient citric acid was added to this precursor solution to obtain a citric acid/$Ce(NO_3)_3{\cdot}6H_2O$ ratio of 3:1. Then, a 5 M NaOH solution was added to the precursor solution dropwise until its pH was 2.5. Half of the prepared solution was transferred to a Teflon vessel and heat treated at 120°C for 14 h in an electric oven; the sample was labeled as S1. The remaining half of the solution was aged at room temperature and subsequently labeled as S2. After sample S1 was heat-treated and sample S2 was aged, both samples were centrifuged twice at 4000 r/min to wash and collect the precipitates. Both precipitates were dried at 80°C in an electric oven overnight and subsequently ground into powders. These powdered samples were then annealed at 300°C for 3 h to obtain the CeO_2 nanostructures. The crystallinity, morphology, optical bandgap, and magnetic properties of the synthesized samples were examined using X-ray diffraction (XRD), scanning electron microscopy (SEM), UV–visible absorption spectroscopy, and vibrating-sample magnetometry (VSM), respectively.

2.2. Determination of antibacterial activity

The interaction of nanomaterials with bacterial surfaces is a pivotal tool for the assessment of antibacterial activity. In the present study, the antibacterial activity of the synthesized CeO_2 nanostructures against clinically isolated Gram-negative *Escherichia coli* (*E. coli*) and Gram-positive methicillin-resistant *Staphylococcus aureus* (*S. aureus*) bacteria was determined by the reported previously agar disc method [17].

3. Results and discussions

3.1. Structural analysis

The structural properties of the prepared CeO_2 nanostructures were investigated by XRD over the 2θ range from 20° to 70° using a small step size (0.2°) and Cu-Kα radiation with a wavelength of 0.154 nm. Fig. 1 illustrates the XRD patterns of the prepared samples. All peaks were well indexed to the pure cubic fluorite-type CeO_2 structure according to JCPDS card no. 34-0394 [18]. The lack of extraneous peaks associated with an impurity in the XRD patterns confirmed the phase purity of the synthesized samples. The broadness of the peaks indicated that the prepared samples are nanocrystalline. Scherrer's formula was used to calculate the crystallite size t, as given by

$$t = \frac{0.89\lambda}{\beta \cos\theta} \tag{1}$$

where λ is the wavelength of incident X-rays, β is the full-width at half-maximum of the selected peak at diffraction angle θ. The crystallite size was determined to be 9 nm for both the hydrothermally treated and the untreated samples. The lattice parameter of each sample was calculated according to the formula

$$d = \frac{a}{\sqrt{h^2 + k^2 + l^2}} \tag{2}$$

where a is lattice constant, d is the interplanar spacing, and h, k, and l are the Miller indices. The lattice parameters of the prepared CeO_2 samples were determined to be 0.5426 nm and 0.5427 nm for samples S1 and S2, respectively. These observed lattice parameters are larger than that of bulk CeO_2 (0.54113 nm). Such variations of the lattice parameter of nanostructured CeO_2 have been attributed to increased oxygen vacancies [19].

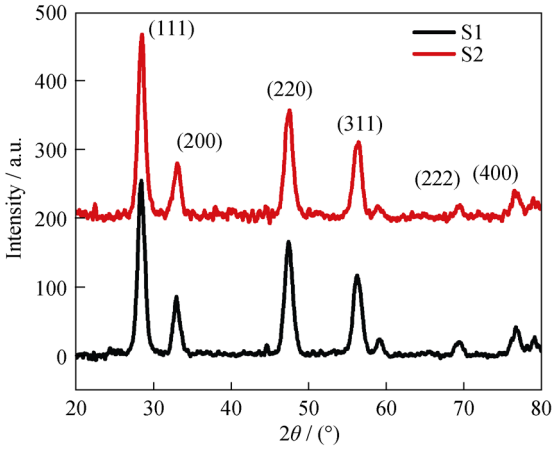

Fig. 1. XRD patterns of synthesized samples.

We used Raman spectroscopy to further investigate the structural characteristics of the synthesized samples. Fig. 2 presents typical Raman spectra of both samples in the range from 300 to 800 cm^{-1} recorded under ambient conditions. In general, the peak (F_{2g} peak) at 443–465 cm^{-1} was attributed to a first-order symmetrical stretching mode of the Ce–O_8 vibration unit. The appearance of a Raman peak at approximately 446 cm^{-1} confirmed the cubic fluorite structure of the prepared samples. The F_{2g} peak was slightly red-shifted in comparison to that of bulk CeO_2. This shift is attributed to disorder in the oxygen sublattice resulting from the smaller particle size. The differences between the spectrum of the synthesized sample and that

of bulk CeO_2 are also attributable to oxygen vacancies [18]. Furthermore, a minor peak was observed at approximately 600 cm^{-1} in the spectrum of the hydrothermally treated sample; this peak is associated with the presence of oxygen vacancies [20]. Hence, the hydrothermally treated sample contained oxygen vacancies, whereas the untreated sample did not.

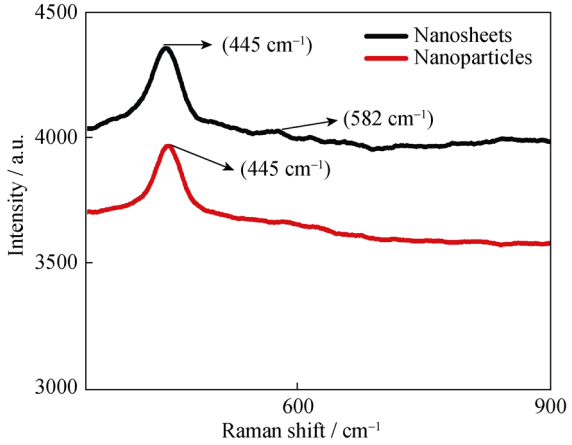

Fig. 2. Raman spectra of prepared CeO_2 nanosheets and nanoparticles.

3.2. Morphology and chemical composition studies

The morphology of the prepared samples was observed by SEM. Fig. 3 presents SEM micrographs of the prepared samples. As evident in Figs. 3(a) and 3(b), the morphology of sample S1 consisted of microspheres composed of highly homogeneous multilayer nanosheets with an average thickness of approximately 40 nm. In comparison, the morphology of sample S2 consisted of spherical nanoparticles with an average size of approximately 30 nm, as shown in Figs. 3(c) and 3(d). A growth mechanism of the synthesized CeO_2 nanostructures is proposed in Fig. 4.

The chemical composition of the prepared CeO_2 nanostructures was determined using energy-dispersive X-ray spectroscopy (EDS); the results are shown in Fig 5. The EDS spectra clearly indicated that only Ce and oxygen (O) ions were present in both CeO_2 nanostructures.

3.3. Optical properties

The optical properties of the prepared CeO_2 nanostructures were examined by UV–visible spectrophotometry. Fig. 6(a) shows the UV–visible absorption spectra of the prepared CeO_2 nanostructures; the spectra of both samples feature a sharp absorption peak at 312 nm, which confirms that the prepared nanostructures possess the cubic fluorite structure [21]. The charge-transfer transition from the O 2p to the Ce 4f states is responsible for the characteristic absorption of CeO_2 in the UV region [22]. The following expression was used to determine the approximate bandgap energy of the synthesized nanostructures:

$$(\alpha h\nu)^2 = A(h\nu - E_g) \tag{3}$$

where α represents the optical absorption coefficient, E_g is the direct-bandgap energy, $h\nu$ is the photon energy, and A is a constant [23].

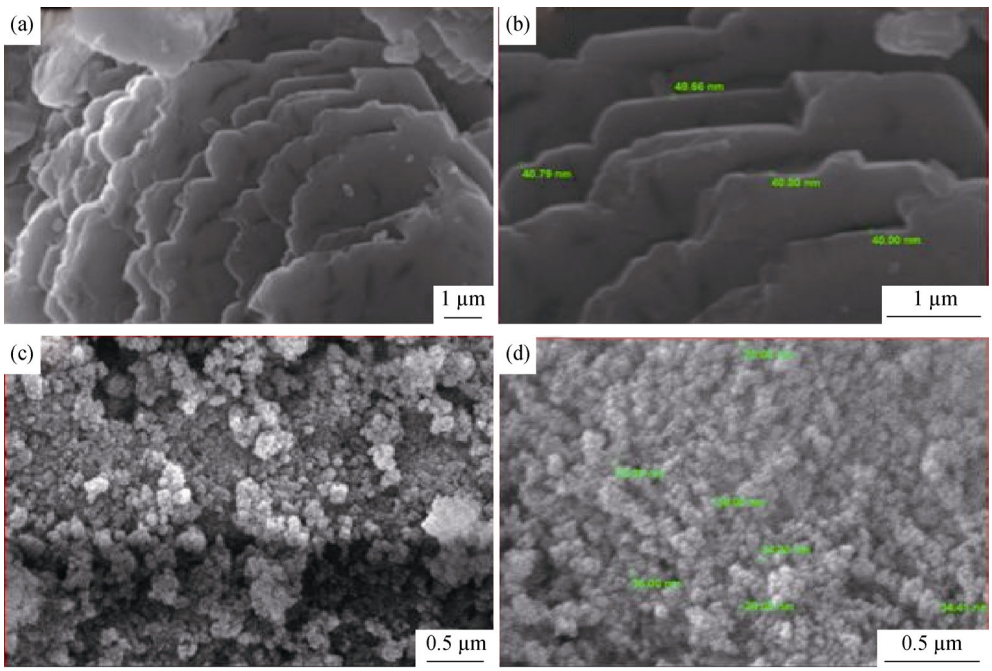

Fig. 3. SEM images of prepared CeO_2 nanostructures: (a, b) S1; (c, d) S2.

Fig. 4. Illustration of the growth mechanism of CeO_2 nanostructures.

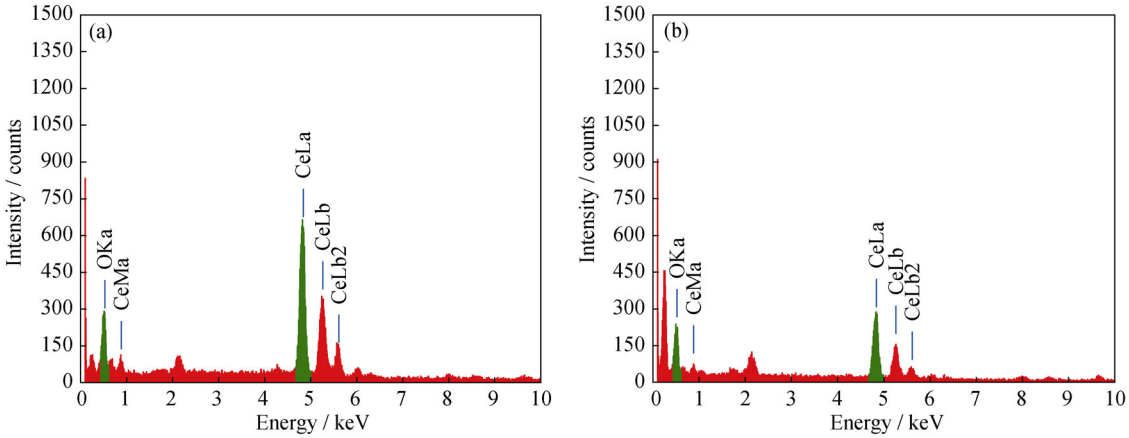

Fig. 5. EDS spectra of prepared CeO_2 nanosheets (a) and nanoparticles (b).

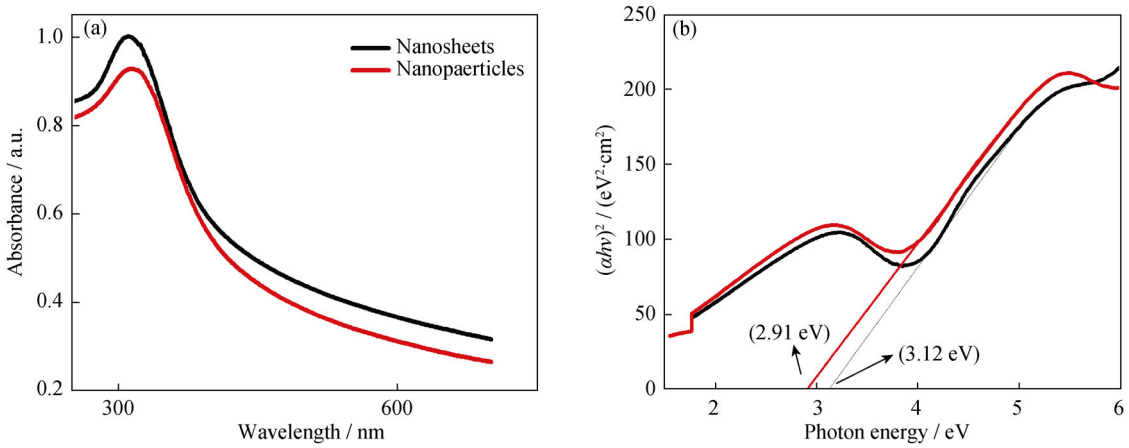

Fig. 6. (a) UV–Vis absorption spectra of synthesized CeO_2 nanostructures; (b) respective plots of $(\alpha h\nu)^2$ as a function of photon energy.

Fig. 6(b) displays the measured values of $(\alpha hv)^2$ as a function of the incident photon energy hv. The direct-bandgap energy of nanostructures can be estimated by extrapolating the straight region of the resulting curve to the energy axis [22].

The results in Fig. 6(b) indicate that the bandgap energies of the prepared CeO_2 nanostructures ere 3.12 eV and 2.91 eV for samples S1 and S2, respectively. These observed energy bandgap values are less than that of bulk CeO_2 (3.20 eV) [22], exhibiting a red shift of 0.08 eV and 0.29 eV, respectively, for the two samples. This red shift of the bandgap energy of the CeO_2 nanostructures is attributable to surface and interface effects [24].

3.4. Magnetic studies

Fig. 7 displays the M–H loops of the prepared CeO_2 nanostructures, as measured by VSM at room temperature. The synthesized microspheres composed of nanosheets (sample S1) exhibit RTFM behavior, whereas the CeO_2 nanoparticles (sample S2) exhibited paramagnetic behavior. In the M–H loop of sample S1, a wide-open hysteresis loop (shown in inset) is observed in the field oscillating in the range of ±1 T. Furthermore, the prepared nanostructures exhibit hysteresis, with a saturated magnetization (M_s) of 0.0068 A·m^2/kg, a coercivity (H_c) of approximately 0.0120 T, and a remanence (M_r) of 0.0019 A·m^2/kg. The RTFM of CeO_2 nanostructures is usually linked to two factors: particle size and the presence of oxygen vacancies [12–13]. As evident from the SEM images, the average particle size of S2 is smaller than that of S1, but S2 still exhibits paramagnetic behavior. Hence, particle-size-induced RTFM is ruled out here. Some other groups have also reported that oxygen vacancies mediate RTFM in undoped semiconducting and insulating oxide nanostructures [12, 19, 24]. The oxygen vacancies formed in the interior of CeO_2 nanostructures easily migrate to the surface and can polarize the Ce 4f electrons [25]. This polarization leads to a net magnetic moment and, hence, to RTFM in CeO_2 nanosheets. The peak at 596 cm^{-1} in the Raman spectrum of the synthesized CeO_2 nanosheets corresponds to oxygen vacancies. The nanomaterials exhibit a high surface area, which may lead to a greater concentration of oxygen vacancies at their surface. Oxygen vacancies at the surface contribute more to the magnetic moment than those in the bulk [12]. These oxygen vacancies at the surface of CeO_2 nanosheets produce spin polarization of the f electrons of CeO_2, which leads to a net magnetic moment [12, 26]. Hence, the RTFM of the CeO_2 nanosheets is attributed to the presence of oxygen vacancies.

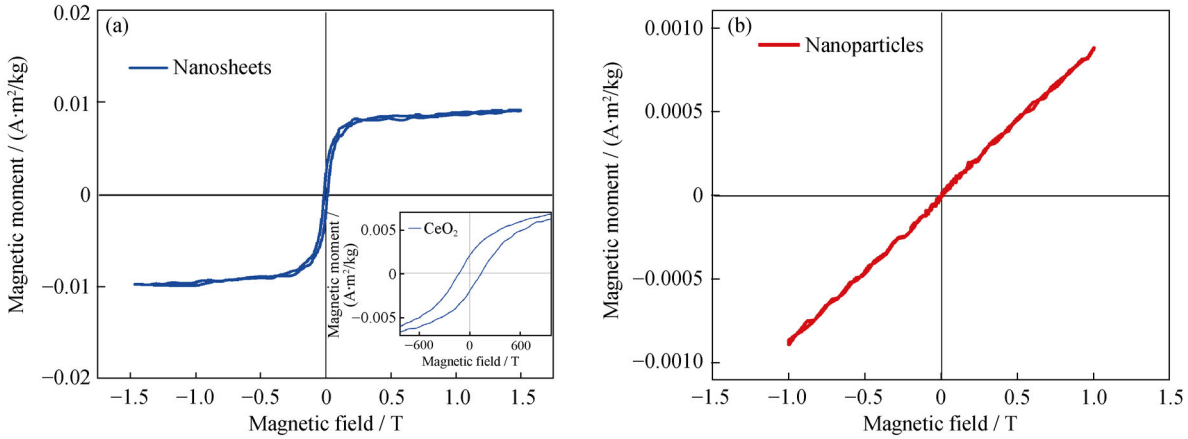

Fig. 7. M–H loops of prepared CeO_2 nanostructures (the inset shows an enlarged view of the opened loops): (a) nanosheets; (b) nanoparticles.

3.5. Antibacterial Activity

The agar disc method is a versatile method for studying antibacterial activity and has been used by several research groups [27–28]. In this work, the antibacterial potency of the synthesized nanostructures against multi-drug resistant *E. coli* and *S. aureus* bacteria was assessed by the agar disc method. The antibacterial potency of materials is demonstrated by the size of the zone of inhibition (ZOI) around the disc. Fig. 8 clearly shows that sample S1 exhibited greater antibacterial activity than S2 against both of the tested bacterial strains. Sample S1 generated a larger ZOI compared to that generated by S2. Several mechanisms of interaction can occur between nanostructures and bacteria cells, such as electrostatic interactions, attachment of the nanostructures to bacteria cell walls, release of soluble metal ions, redox reactions, and the generation of reactive oxygen species (ROS). The generation of ROS is highly dependent on the inhibition of the recombination of photogenerated electron–hole pairs. The oxygen vacancies can

trap the generated electrons and reduce their likelihood of recombining with holes [29]. These holes, in turn, interact with the water molecules and generate ROS. The generated ROS react harmfully with the bacteria and cause their death. Hence, the greater antibacterial activity of the synthesized nanosheets is attributable to the enhanced generation of ROS due to the presence of oxygen vacancies.

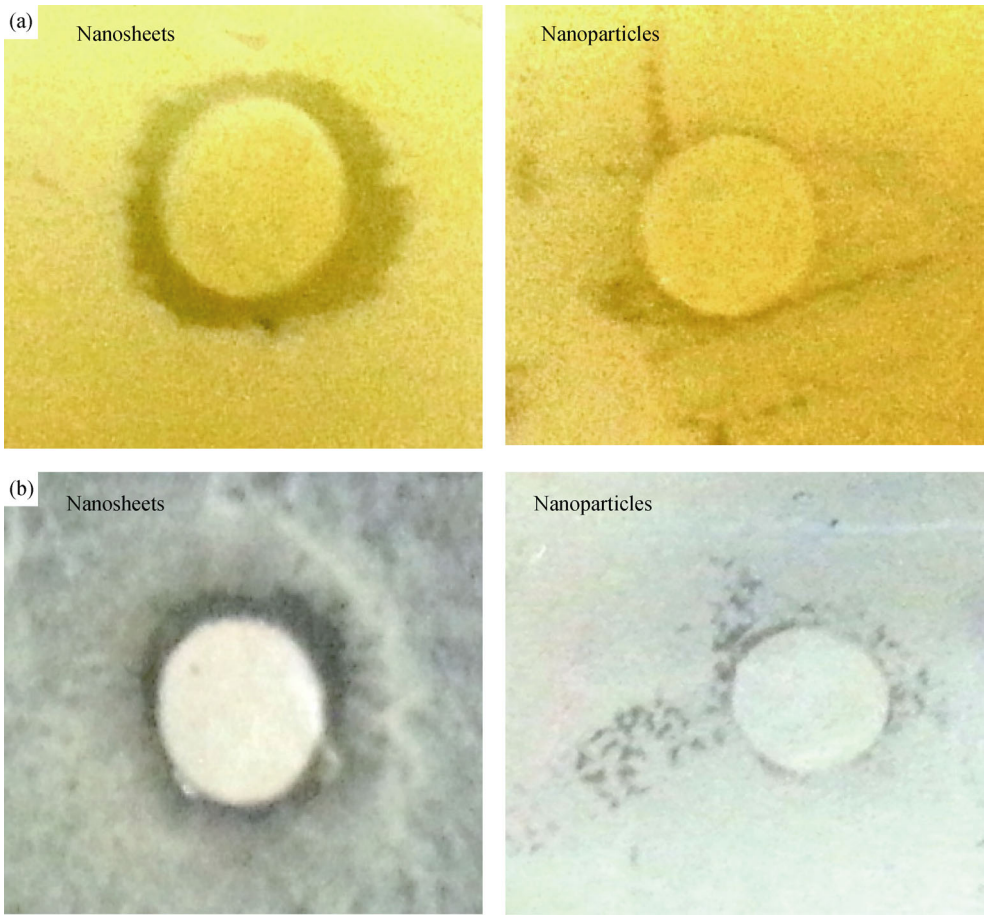

Fig. 8. ZOI produced by the prepared CeO_2 nanostructures against *E. coli* (a) and *S. aureus* (b).

4. Conclusions

(1) CeO_2 nanostructures with the cubic fluorite structure were successfully synthesized by a soft chemical method.

(2) The XRD and Raman results confirmed that the CeO_2 consisted of a single phase. The Raman results further suggested the presence of a large number of oxygen vacancies in the CeO_2 nanosheets.

(3) SEM micrographs revealed the formation of microspheres composed of nanosheets in the hydrothermally treated sample and the formation of nanoparticles in the untreated sample.

(4) The optical bandgap energies of the hydrothermally treated and untreated samples were determined to be 3.12 eV and 2.91 eV, respectively.

(5) The prepared CeO_2 nanosheets exhibited RTFM, which we attributed to the presence of oxygen vacancies on the surface; the CeO_2 nanoparticles exhibited paramagnetic behavior.

(6) The results of antibacterial activity tests demonstrated that the prepared CeO_2 nanosheets exhibit high antibacterial activity compared with the CeO_2 nanoparticles, which we attributed to the enhanced generation of ROS in the CeO_2 nanosheets.

Acknowledgements

This work is funded by the Higher Education Commission of Pakistan (HEC) IPFP (Grant No. PM-IPFP/HRD/HEC/2011/3386) to Dr. Javed Iqbal Saggu and funding for HEC Ph.D. Scholar (Tariq Jan) under his supervision.

Ethical statement(s)

The authors report no conflict of interest in this work.

References

[1] X.J. Yu, P.B. Xie, and Q.D. Su, Size-dependent optical properties of nanocrystalline CeO_2:Er obtained by combustion synthesis, *Phys. Chem. Chem. Phys*., 3(2011), p. 5266.

[2] C.H. Hu, C.H. Xia, F. Wang, M. Zhou, P.F. Yin, and X.Y. Han, Synthesis of Mn-doped CeO_2 nanorods and their application as humidity sensors, *Bull. Mater. Sci*., 34(2011), No. 5, p. 1033.

[3] V. Shah, S. Shah, H. Shah, F.J. Rispoli, K.T. McDonnell, S. Workeneh, A. Karakoti, A. Kumar, and S. Seal, Antibacterial activity of polymer coated cerium oxide nanoparticles, *Plos One*, 7(2012), No. 10, p. e47827.

[4] A.I.Y. Tok, F.Y.C. Boey, Z. Dong, and X.L. Sun, Hydrothermal synthesis of CeO_2 nano-particles, *J. Mater. Process. Technol.*, 190(2007), No. 1-3, p. 217.

[5] I. Celardo, J.Z. Pedersen, E. Traversa, and L. Ghibelli, Pharmacological potential of cerium oxide nanoparticles, *Nanoscale*, 3(2011), p. 1411.

[6] F.M. Meng, L.N. Wang, and J.B. Cui, Controllable synthesis and optical properties of nano-CeO_2 via a facile hydrothermal route, *J. Alloys Compd.*, 556(2013), p. 102.

[7] C. Zhang, F.M. Meng, L.N. Wang, M. Zhang, and Z.L. Ding, Morphology-selective synthesis method of gear-like CeO_2 microstructures and their optical properties, *Mater. Lett.*, 130(2014), p. 202.

[8] N.S. Arul, D. Mangalaraj, P.C. Chen, N. Ponpandian, P. Meena, and Y. Masuda, Enhanced photocatalytic activity of cobalt-doped CeO_2 nanorods, *J. Sol Gel Sci. Technol.*, 64(2012), No. 3, p. 515.

[9] S. Atiq, S.A. Siddiqi, F. Abbas, M. Saleem, and S.M. Ramay, Carriers-assisted enhanced ferromagnetism in Al-doped ZnMnO nano-crystallites, *Chin. J. Chem. Phys.*, 26(2013), No. 4, p. 457.

[10] J. Iqbal, T. Jan, R.H. Yu, S.H. Naqvi, and I. Ahmad, Doping induced tailoring in the morphology, band-gap and ferromagnetic properties of biocompatible ZnO nanowires, nanorods and nanoparticles, *Nano Micro Lett*., 6(2014), No. 3, p. 242.

[11] M.I.B. Bernardi, A. Mesquita, F. Béron, K.R. Pirota, A.O. de Zevallos, A.C. Doriguettod, and H.B. de Carvalho, The role of oxygen vacancies and their location in the magnetic properties of $Ce_{1-x}Cu_xO_{2-\delta}$ nanorods, *Phys. Chem. Chem. Phys*., 17(2015), p. 3072.

[12] M.Y. Ge, H. Wang, E.Z. Liu, J.F. Liu, J.Z. Jiang, Y.K. Li, Z.A. Xu, and H.Y. Li, On the origin of ferromagnetism in CeO_2 nanocubes, *Appl. Phys. Lett*., 93(2008), No. 6, p. 062505.

[13] Y.L. Liu, Z. Lockman, A. Aziz, and J. MacManus-Driscoll, Size dependent ferromagnetism in cerium oxide (CeO_2) nanostructures independent of oxygen vacancies, *J. Phys. Condens. Matter.*, 20(2008), No. 16, p. 165201.

[14] S.B. Ogale, R.J. Choudhary, J.P. Buban, S.E. Lofland, S.R. Shinde, S.N. Kale, V.N. Kulkarni, J. Higgins, C. Lanci, J.R. Simpson, N.D. Browning, S.D. Sarma, H.D. Drew, R.L. Greene, and T. Venkatesan, High temperature ferromagnetism with a giant magnetic moment in transparent Co-doped $SnO_{2-\delta}$, *Phys. Rev. Lett*., 91(2003), No. 7, p. 077205-1.

[15] L.N. Wang and F.M. Meng, Oxygen vacancy and Ce^{3+} ion dependent magnetism of monocrystal CeO_2 nanopoles synthesized by a facile hydrothermal method, *Mater. Res. Bull.*, 48(2013), No. 9, p. 3492.

[16] Q.H. Bo, F.M. Meng, and L.N. Wang, Facile hydrothermal synthesis of CeO_2 nano-octahedrons and their magnetic properties, *Mater. Lett.*, 133(2014), p. 216.

[17] T. Jan, J. Iqbal, M. Ismail, M. Zakaullah, S.H. Naqvi, and N. Badshah, Sn doping induced enhancement in the activity of ZnO nanostructures against antibiotic resistant *S. aureus* bacteria, *Int. J. Nanomed.*, 8(2013), p. 3679.

[18] M. Li, R. Zhang, H. Zhang, W. Feng, and X. Liu, Synthesis, structural and magnetic properties of CeO_2 nanoparticles, *Micro Nano Lett.*, 5(2010), No. 2, p. 95.

[19] A. Thurber, K.M. Reddy, V. Shutthanandan, M.H. Engelhard, C. Wang, J. Hays, and A. Punnoose, Ferromagnetism in chemically synthesized CeO_2 nanoparticles by Ni doping, *Phys. Rev. B*., 76(2007), p. 165206.

[20] S. Phoka, P. Laokul, E. Swatsitang, V. Promarak, S. Seraphin, and S. Maensiri, Synthesis, structural and optical properties of CeO_2 nanoparticles synthesized by a simple polyvinyl pyrrolidone (PVP) solution route, *Mater. Chem. Phys*., 115(2009), No. 1, p. 423.

[21] S.B. Khan, M. Faisal, M.M. Rahman, and A. Jamal, Exploation of CeO_2 nanoparticles as a chemi-sensor and photo-catalyst for environmental applications, *Sci. Total Environ*., 409(2011), No. 15, p. 2987.

[22] H. Imagawa and S.H. Sun, Controlled synthesis of monodisperse CeO_2 nanoplates developed from assembled nanoparticles, *J. Phys. Chem. C*, 116(2012), No. 4, p. 2761.

[23] E. Ziegler, A. Heinrich, H. Oppermann, and G. Stöver, Electrical properties and non-stoichiometry in ZnO single crystals, *J. Phys. Status Solidi A*, 66(1981), No. 2, p. 635.

[24] S. Phokha, S. Pinitsoontorn, and S. Maensiri, Room-temperature ferromagnetism in Co-doped CeO_2 nanospheres prepared by the polyvinylpyrrolidone-assisted hydrothermal method, *J. Appl. Phys.*, 112(2012), p. 113904.

[25] L.J. Wu, H.J. Wiesmann, A.R. Moodenbaugh, R.F. Klie, Y.M. Zhu, D.O. Welch, and M. Suenaga, Oxidation state and lattice expansion of CeO_{2-x} nanoparticles as a function of particle size, *Phys. Rev. B*., 69(2004), p. 125415.

[26] N.H. Hong, J. Sakai, and F. Gervais, Magnetism due to oxygen vacancies and/or defects in undoped semiconducting and insulating oxide thin films, *J. Magn. Magn. Mater*., 316(2007), No. 2, p. 214.

[27] R.R. Gandhi, S. Gowri, J. Suresh, and M. Sundrarajan, Ionic liquids assisted synthesis of ZnO nanostructures: controlled size, morphology and antibacterial properties, *J. Mater. Sci. Technol*., 29(2013), No. 6, p. 533.

[28] T. Jan, J. Iqbal, M. Ismail, and A. Mahmood, Synthesis of highly efficient antibacterial agent Ag doped ZnO nanorods: structural, Raman and optical properties, *J. Appl. Phys*., 115(2014), p. 154308.

[29] T. Jan, J. Iqbal, Q. Mansoor, M. Ismail, M.S.H. Naqvi, A. Gul, S.F.H. Naqvi, and F. Abbas, Synthesis, physical properties and antibacterial activity of Ce doped CuO: a novel nanomaterial, *J. Phys. D*, 47(2014), No. 35, p. 355301.